3D Weaving with Curved Ribbons

YINGYING REN, EPFL, Switzerland
JULIAN PANETTA, UC Davis, USA
TIAN CHEN, EPFL, Switzerland
FLORIN ISVORANU, EPFL, Switzerland
SAMUEL POINCLOUX, EPFL, Switzerland
CHRISTOPHER BRANDT, EPFL, Switzerland
ALISON MARTIN, Weaver and Independent Researcher, Italy
MARK PAULY, EPFL, Switzerland

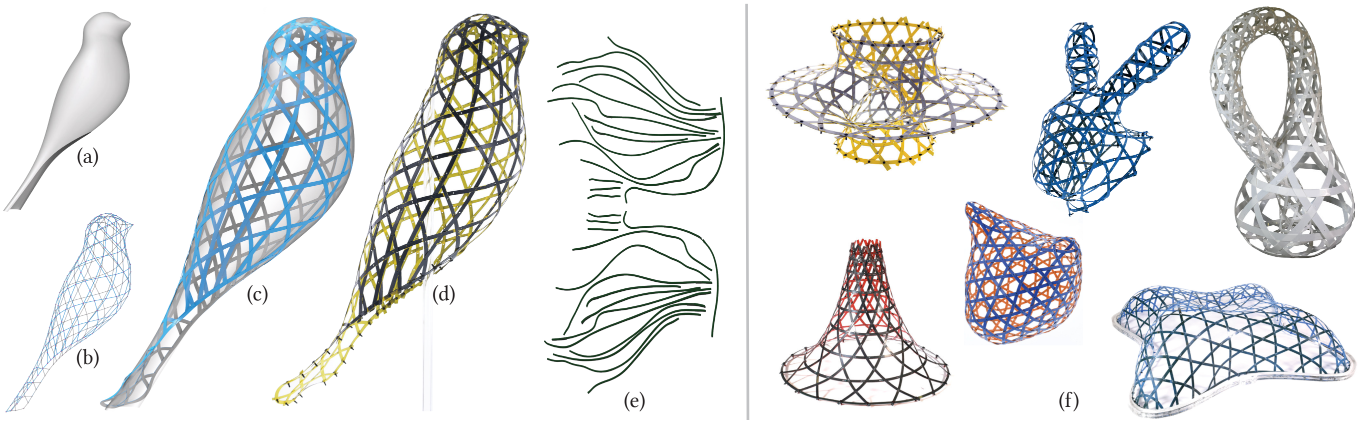

Fig. 1. Our inverse design optimization algorithm takes as input a target design surface (a) and a weaving topology graph (b), and calculates the planar freeform ribbon shapes (e) so that the simulated equilibrium weave (c) and final physical prototype (d) best approximate the target surface. Several fabricated models illustrate how our method allows weaving a variety of double-curved surfaces from planar curved ribbons (f).

Basket weaving is a traditional craft for creating curved surfaces as an interwoven array of thin, flexible, and initially straight ribbons. The three-dimensional shape of a woven structure emerges through a complex interplay of the elastic bending behavior of the ribbons and the contact forces at their crossings. Curvature can be injected by carefully placing topological singularities in the otherwise regular weaving pattern. However, shape control through topology is highly non-trivial and inherently discrete, which severely limits the range of attainable woven geometries. Here, we demonstrate how to construct arbitrary smooth free-form surface geometries by weaving carefully optimized *curved* ribbons. We present an optimization-based approach to solving the inverse design problem for such woven structures. Our algorithm computes the ribbons' planar geometry such that their interwoven assembly closely approximates a given target design surface in equilibrium. We systematically validate our approach through a series of physical prototypes to show a broad range of new woven geometries that is not achievable by existing methods. We anticipate our computational approach to significantly enhance the capabilities for the design of new woven structures. Facilitated by modern digital fabrication technology, we see potential applications in material science, bio- and mechanical engineering, art, design, and architecture.

CCS Concepts: • **Computing methodologies → Shape Modeling**; **Simulation**.

Additional Key Words and Phrases: weaving, physics-based simulation, numerical optimization, computational design, fabrication

ACM Reference Format:
Yingying Ren, Julian Panetta, Tian Chen, Florin Isvoranu, Samuel Poincloux, Christopher Brandt, Alison Martin, and Mark Pauly. 2021. 3D Weaving with Curved Ribbons. *ACM Trans. Graph.* 40, 4, Article 127 (August 2021), 15 pages. https://doi.org/10.1145/3450626.3459788

1 INTRODUCTION

Weaving is a fundamental principle for assembling linear material elements through interlacing to form stable compound 2D or 3D

Authors' addresses: Y. Ren, EPFL, yingying.ren@epfl.ch; J. Panetta, UC Davis, julian.panetta@gmail.com; T. Chen, EPFL, tian.chen@epfl.ch; F. Isvoranu, EPFL, florin.isvoranu@epfl. ch; S. Poincloux, EPFL, samuel.poincloux@epfl.ch; C. Brandt, EPFL, christopher.brandt.n@gmail.com; A. Martin, Private, alisonmartin57@gmail.com; M. Pauly, EPFL, mark.pauly@epfl.ch.

Permission to make digital or hard copies of all or part of this work for personal or classroom use is granted without fee provided that copies are not made or distributed for profit or commercial advantage and that copies bear this notice and the full citation on the first page. Copyrights for components of this work owned by others than the author(s) must be honored. Abstracting with credit is permitted. To copy otherwise, or republish, to post on servers or to redistribute to lists, requires prior specific permission and/or a fee. Request permissions from permissions@acm.org.
© 2021 Copyright held by the owner/author(s). Publication rights licensed to ACM.
0730-0301/2021/8-ART127 $15.00
https://doi.org/10.1145/3450626.3459788

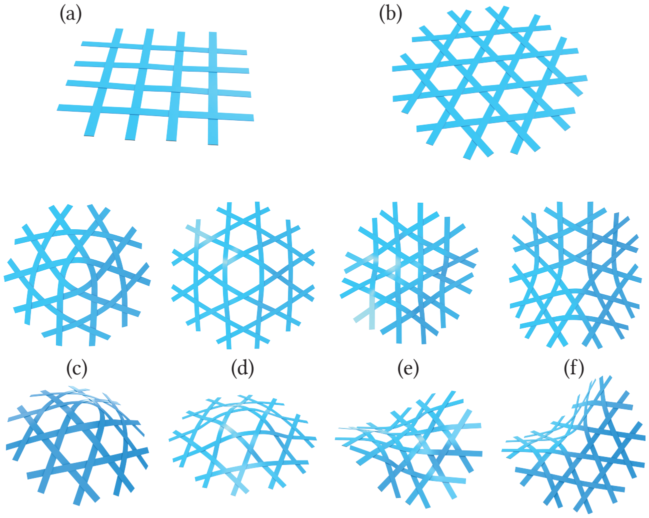

Fig. 2. Traditional weaving with straight ribbons mainly employs the biaxial pattern (a) or the triaxial (Kagome) pattern (b). Non-zero Gaussian curvature leads to the irregular spacing of ribbons (d,e). Alternatively, topological singularities allow introducing positive (c) or negative (f) Gaussian curvature while keeping the spacing more uniform.

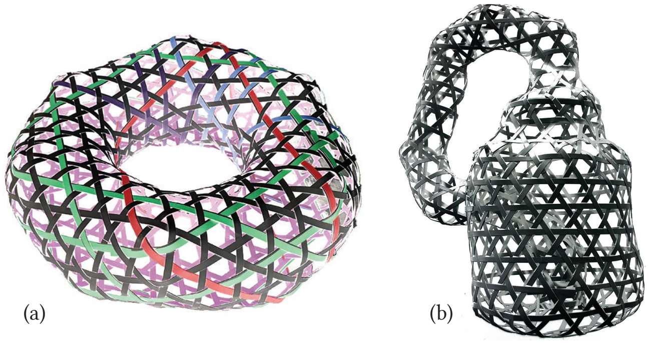

Fig. 3. Topological distortions concentrate curvature locally, which can lead to deviations from the desired target geometry and a "blocky" appearance when trying to approximate a smooth torus (a) or Klein bottle (b). Artworks by Alison Martin.

structures. Widely observed in nature, for example, in the construction of bird nests [Hansell and Overhill 2000], weaving is a traditional craft in many cultures and finds broad application in textiles, art, decorative objects, household items, or architectural design [Albers et al. 2017; Ayres et al. 2020]. Modern industrial processes use weaving with novel synthetic materials to produce structures of unique functionalities and exceptional strength [Lewandowska et al. 2017; Rana and Fangueiro 2015].

Here, we focus on weaving with elastic ribbons to form 3D surface structures. Commonly referred to as *basket weaving*, this process traditionally interleaves straight ribbons in regular patterns with alternating over- and under-crossings to obtain a stable lattice structure. Most prominently, the biaxial and triaxial (Kagome) patterns interleave two resp. three families of parallel ribbons as illustrated in Figure 2. Topological singularities are added to inject curvature locally, typically in a few carefully selected locations, for example to produce corners in a basket (see also Figure 3).

In this paper, we generalize the traditional process of basket weaving using straight ribbons to arbitrarily *curved* ribbons and show how this generalization significantly enlarges the range and quality of attainable shapes. On the other hand, determining the optimal curved shape of each individual ribbon in a globally coupled woven structure is highly non-trivial and typically beyond the capabilities of human designers. We therefore propose a computational design approach for curved weaving.

Contributions. The core contribution of this paper is a computational pipeline for the inverse design of woven structures using curved planar ribbons. The key algorithmic novelty is a multi-stage optimization method to solve for the freeform 2D rest shape of the ribbons such that the equilibrium state of their woven ensemble best approximates a given input surface. We show how a novel ribbon crossing model allows optimizing the contact forces acting on interlaced ribbons to improve the stability of the woven structure. Our approach enables the weaving of complex freeform surfaces that cannot be handled by any existing method. We validate our optimization method through a series of physical prototypes that show excellent agreement with the simulation prediction.

2 RELATED WORK

Our work fits into a recent line of research on fabrication-aware design [Bermano et al. 2017; Pietroni et al. 2019]. In this section, we briefly summarize literature that is more broadly related to our research. We then discuss previous work on weaving in section 3 after we define certain concepts and terminology.

The general goals of fabrication-aware computational design are to provide effective means for design exploration under constraints imposed by a chosen material system and / or manufacturing method and to produce functional objects that optimize user-specified objectives. The design space of such problems often involves geometric, material, and fabrication parameters.

Numerous research works have proposed inverse design optimization approaches to transform or assemble fabricated components to produce a target design surface. Examples include origami [Dudte et al. 2016], kirigami [Choi et al. 2019; Jiang et al. 2020], curved folding [Kilian et al. 2017], zippables [Schüller et al. 2018], auxetics [Konaković et al. 2016; Konaković-Luković et al. 2018], pneumatic elastomers [Siéfert et al. 2019], or hydrogels [Gladman et al. 2016]. Similar to our work, these methods often combine geometric abstractions of material properties with physical simulation to enable accurate predictions of the final produced model.

In a similar vein, various curve-based material systems for shape approximation have been studied in the past. Miguel et al. [2016] present a computational method for designing wire sculptures fabricated using a 2D wire bending machine. Garg and colleagues [2014] presented a computational design approach for wiremeshes — regular interwoven elastic threads that are inextensible but allow shearing within the lattice. They show how discrete Chebyshev nets can be used to design an interactive, optimization-supported design tool for approximating freeform surfaces by single wiremesh patches. Sageman-Furnas et al. [2019] propose a more general approach based on poly-vector fields that can also handle singularities to increase the range of attainable shapes. The works of [Guseinov et al. 2017] and [Pérez et al. 2017] presented an actuated system that has carefully optimized curve elements embedded onto a stretched fabric and deploys towards a desired target shape as the elastic energy of the fabric is released.

The design and fabrication of curve networks on surfaces have been studied by [Chen et al. 2016; Pérez et al. 2015; Zehnder et al. 2016]. In these works, discrete curve representations are used to simulate and optimize the layout of structural or ornamental curves on a surface that can be 3D printed as a monolithic structure. Situated between sheet- and rod-based systems, [Malomo et al. 2018] build upon this work and present an inverse design method to optimize the layout and geometry of spiral elements to conform to a quad-mesh representation of the design surface. Elastic curve modeling also finds application in meshing. For example, [Campen and Kobbelt 2014] propose an interactive method for designing quad mesh layouts by optimizing dual loops embedded in the surface modeled as Euler elastica.

Deng and co-workers [2011] studied curve networks on freeform surfaces at the architectural scale. They relate certain advantages in fabrication and assembly to geometric curve properties. In particular, curves that follow geodesics, lie in planes intersecting the surface, or can be composed of circular arcs are shown to be beneficial for construction. In our setting, we are not limited to specific geometric sub-classes of curve networks and directly optimize the curvature of ribbons while taking into account their elastic deformation behavior.

3 WEAVING

We assume our ribbons are cut from flat, flexible material of constant thickness[1]. We further expect that the material is significantly thinner than the width of a ribbon so that ribbons easily twist and bend along their weak axis but prohibit significant bending along their stiff axis.

Figure 2(a,b) shows the two predominant weaving patterns, the biaxial and the triaxial (Kagome) weaves. These patterns consist of two or three families of parallel curves at constant spacings. Ribbons form stable weaves through interlacing, alternating between over and under crossings [Behera and Hari 2010]. This alternation causes the ribbons to bend in such a way that they exert compressive forces onto each other, which induces sufficient friction forces to hold the ribbons in place.

3.1 Weaving with Straight Ribbons

Planar weaves with straight ribbons based on the biaxial or triaxial pattern can be deformed relatively easily to approximate developable surfaces, as this mainly induces deformations of the ribbons along their weak axis. The ribbons will then approximately follow geodesic curves on the surface [Pottmann et al. 2010].

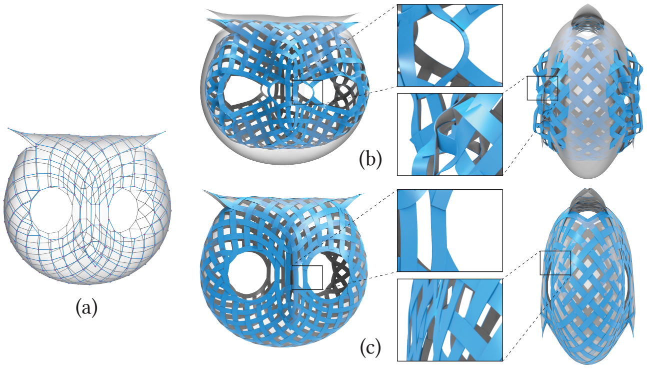

Fig. 4. For a pre-defined topology (a), weaving with straight ribbons can incur significant twisting and buckling (b), which leads to a large deviation from the desired target surface. Our optimized curved ribbons (c) assume an equilibrium state that closely approximate the target.

When moving towards surfaces with non-zero Gaussian curvature, the regular pattern gradually distorts as ribbons follow the deforming geodesics, and variations in the spacing of neighboring ribbons emerge (Figure 2(d, e)). As curvature increases, two neighboring ribbons can eventually collide. To avoid interpenetration and maintain even spacings, we must free the ribbons from following geodesics. For straight ribbons, this means twisting so that the flexible bending deformation mode can produce geodesic curvature (not just normal curvature). Such twisting, however, is problematic for weaving, mainly because ribbons no longer lie flat upon each other at crossings. This leads to undesirable local deformations, potential stress concentrations in the ribbons, and insufficient frictional contact, which can compromise the stability and visual appearance of the woven structure (see also Figure 4).

An alternative approach to allow deviating from developable surfaces is to introduce topological distortions into the weaving pattern. These singularities allow restructuring the ribbons locally, so ribbons can switch from one family to another. Effectively, this injects curvature locally into the woven structure as illustrated in Figure 2(c, f). In traditional weaving, the placement and type of singularity are typically determined empirically based on the intuition and experience of the designer [Ayres et al. 2018]. Recently, Vekhter and colleagues [Vekhter et al. 2019] proposed an optimization algorithm for straight ribbon weaving. Using a suitable discretization of the geodesic equation, they compute geodesic foliations on branched covers of the design surface to produce a complete weaving pattern with automatically placed singularities. While this is an effective solution for straight ribbons, inverse design with curved ribbons can no longer rely on geodesic fields and thus requires a fundamentally different approach.

Direct modeling approaches for straight ribbon weaving have also been explored, for example using procedural modeling [Kaplan and Cohen 2003] or shape grammars [Fajar and Indraprastha 2016]. The work of [Tao et al. 2017] and [Igarashi 2019] presented interactive systems for novice users to design simple woven geometries based on explicitly modeled parameter curves.

---

[1] Here we only consider ribbons of constant thickness as these can be cut easily from planar sheet material. Our algorithm, however, in principle supports varying material thickness.

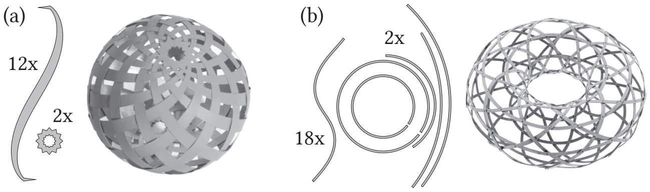

Fig. 5. Curved ribbon weaving has been explored in design using manually drawn ribbon shapes [Schepper and Schepper 2014] (a), and in engineering [Baek et al. 2020] using parameterized ribbons composed of circular arc segments (b).

Recent work on deployable beam networks [Panetta et al. 2019; Pillwein et al. 2020] have connections to weaving in that they also model networks of bending-active linear elements. In contrast to weaving, these elements are placed on top of each other rather than interleaved and are connected explicitly with joints, which are essential for the structural stability of the deployed structure.

3.2 Weaving with Curved Ribbons

Curved ribbons have been explored in design and engineering as exemplified in Figure 5. The key idea is to inject in-plane curvature into the ribbons' rest shape. As a consequence, ribbons are no longer constrained to follow geodesic paths on the surface, which provides more flexibility to build a regular woven structure.

Singularities in the weaving pattern are still required to satisfy global topological constraints, and they can be helpful to reduce ribbon curvature if desired (see also Figure 15). However, as we show in our results, suitably optimized curved ribbons avoid unfavorable local curvature concentrations and generally lead to a much better approximation of the target shape. In addition, we gain significant freedom in the choice of weaving pattern topology, which is largely decoupled from the geometry of the design surface (see also Figure 16 and Figure 18).

Previous work on curved ribbon weaving was pioneered by Akleman and colleagues [2009] who presented a projection algorithm to compute weaving patterns on surfaces based on graph rotation systems. They show how plain-weavings derived from edge twisting can be converted into 3D thread structures that densely cover a given manifold mesh. This approach has been applied in [Xing et al. 2011] to create a large-scale sculpture. A related geometric strategy has been reported by [Mallos 2009]. These methods are mostly suited for dense weavings, but do not consider the physical deformation behavior of ribbons nor the resulting contact forces at crossings, which are essential in our approach to accurately predict the equilibrium state of our woven structures.

[Baek et al. 2020] propose a unit cell approach for assembling woven structures using a parameterized model for curved ribbons. Each ribbon consists of a combination of straight and circular arcs of fixed length. Varying the arc radius allows adapting the ribbon rest shape to improve shape approximation over traditional weaving. They show how elementary shapes such as spheres, ellipsoids or tori can be created with a manual forward design process. In contrast, our approach supports arbitrarily shaped curved ribbons and algorithmically determines their optimal rest shape to solve the inverse design problem.

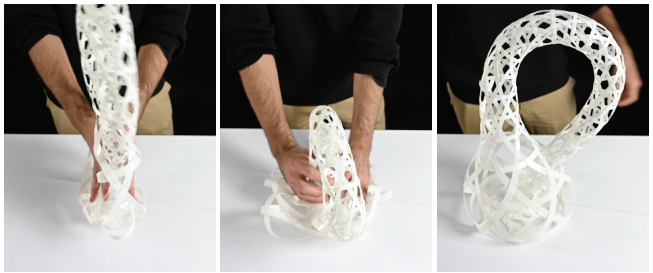

Fig. 6. Even after extreme deformations, the optimized woven model settles back reliably into the predicted equilibrium state.

4 OVERVIEW

A woven structure is a complex coupled system of bending-active elements. Each ribbon experiences external forces due to frictional contacts with other ribbons in the weave, which are balanced by internal forces that arise due to stretching, bending, and twisting of the ribbons (see also Figure 6). As a consequence, a purely geometric approach, for example projecting a smooth curve pattern onto the design surface and unrolling each ribbon onto the plane, in general does not accurately reproduce the input surface. The internal stresses of ribbons are not taken into account, leading to deformations of the woven structure, in particular when ribbons follow curves of high normal curvature on the surface.

To accurately predict the final shape of a woven structure, it is therefore essential to compute the global equilibrium state of the interleaved ribbons through physical simulation. This means that our inverse design algorithm needs to accurately track this equilibrium state while the ribbons' planar rest shapes are optimized.

Figure 7 provides a high-level overview of our optimization approach. Our method takes as input a target design surface S given as a triangle mesh and a graph G that specifies the weave pattern topology. Nodes of G define ribbon crossings and should be embedded in the design surface. These initial crossing positions provide information about the design intent for the weave, but will change during the optimization. The traditional challenge of designing weaving pattern G for straight ribbons is the final shape's reliance on the careful insertion and adjustment of singularities. Allowing ribbons to be curved minimizes the weaving topology's influence on the shape, freeing us to either generate graphs automatically with meshing tools or craft them manually to achieve artistic goals (see also Figure 8 and Figure 16). The graph G is automatically converted into ribbons following the approach outlined in the supplemental material. We assume only two ribbons cross at any location and compute the over-under relationship using a breadth-first search [Mallos 2009].

Our optimization starts from a simple initialization with straight ribbons. Figures 4 and 7 illustrate how these initially straight ribbons exhibit severe buckling and twisting, which would lead to an unstable weave with a large deviation from the target design surface. The optimized curved ribbons closely approximate the target with low elastic energy, leading to a more stable woven structure.

The final stage of the pipeline analyzes contact forces at crossings. If we detect ribbons that are no longer in contact at a crossing, we

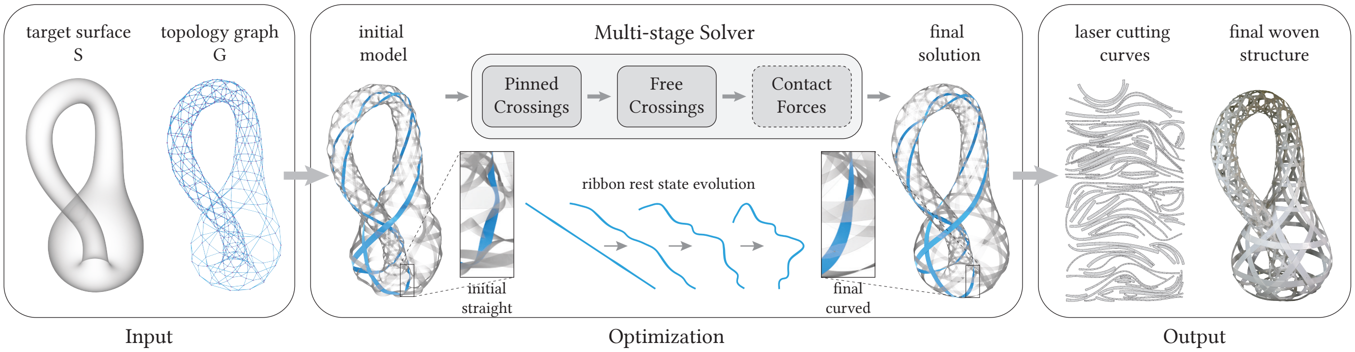

Fig. 7. Our inverse design optimization takes as input a target surface and weaving topology graph and produces as output the 2D cutting paths of the ribbons. The optimization is initialized with straight ribbons and jointly solves for their planar curved rest state and the final equilibrium shape to best approximate the target surface. The final optimization stage of contact forces is only applied if ribbon separation is detected.

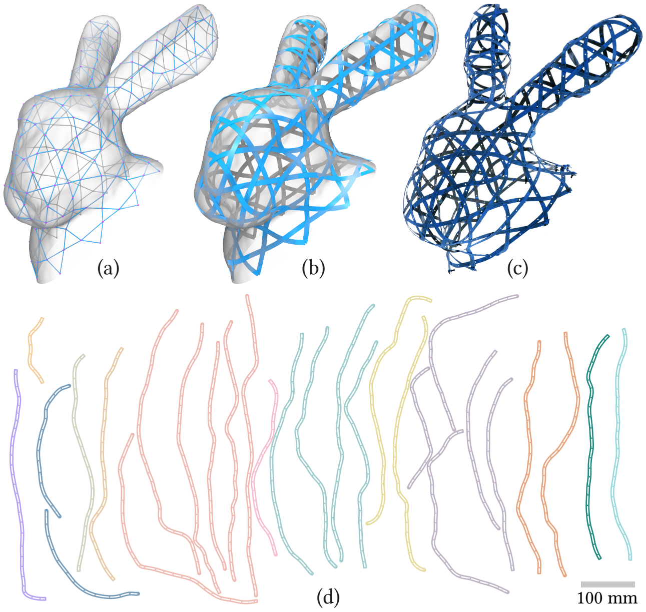

Fig. 8. Input (a), predicted simulation (b), final fabricated model (c), and optimized 2D ribbons (d). Ribbons of the same color originated from a single ribbon that has been split to fit the dimensions of the laser cutting machine and to avoid in-plane self-intersections. These ribbon components are reconnected in the final weaving. The dots indicate ribbon crossing locations. The input topology graph in (a) has been computed automatically using the method of [Jakob et al. 2015].

further optimize the ribbon geometry to ensure stable contacts at the cost of a potentially higher-energy weave or larger deviations from the target surface. Alternatively, we can iteratively modify the over-under relation at selected crossings to reduce separation contact forces, trading off the regularity of the alternation pattern for improved weaving stability (see also Figure 14).

Our inverse design optimization is based on the method proposed by Panetta et al. [2019] for optimizing X-shells — pin-jointed deployable gridshells composed of straight elastic beams. We briefly summarize this approach in section 5 where we introduce our new extended representation for curved ribbon weaving. In section 6, we discuss our formulation of the optimization objective function and introduce new terms specific to our setting. section 7 then presents our multi-stage numerical solver to minimize this objective. We present simulated and fabricated examples in section 8, where we quantitatively analyze our simulation's predictive accuracy.

5 REPRESENTATION

We simulate the deformation behavior of ribbons using the discrete elastic rod model proposed in [Bergou et al. 2010, 2008]. Each ribbon is modeled as a collection of rod segments defined between pairs of consecutive ribbon crossings. A rod segment is represented as a polyline with vertex positions in 3D and an adapted material frame on each edge defining the ribbon orientation. By maintaining reference frames adapted to the polyline edges, this ribbon orientation is expressed with a single material frame angle variable θ. To model the coupling of ribbons at their crossings, we design a special crossing representation that ensures crossing ribbons share a contact point with compatible local orientations by construction and therefore circumvents difficult nonlinear interpenetration constraints (see Figure 9). A crossing's configuration, defined by its angle, position, and orientation variables, is used to set the endpoint positions and ribbon orientations of the incident terminal edges of each participating rod segment.

We augment the straight beam model of [Panetta et al. 2019] by introducing in-plane curvature to the rest configuration of ribbons. These additional design variables are stored as turning angles κ (integrated curvature) at each vertex of the rod polylines. Consequently, the simulation variables in our framework are the *independent* variables for rod position and angle θ (those not set by crossings) combined with the crossing variables in the deformed state. The design variables that we optimize for are the lengths l and discrete curvature values κ of the ribbons in the planar rest state (see Figure 9). We aggregate all simulation variables in a vector $\mathbf{x}$ and all design variables in a vector $\mathbf{p}$. Please refer to our supplemental material for more details of the representation.

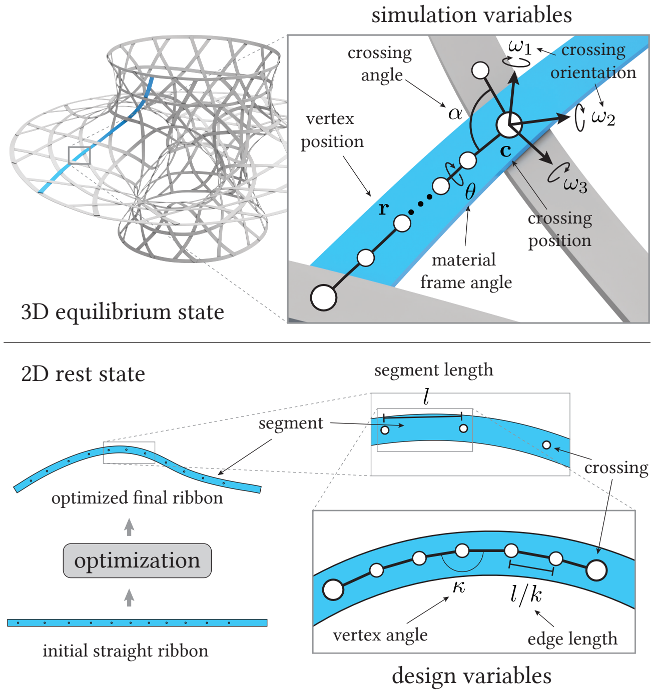

Fig. 9. A ribbon is composed of several elastic rod segments, each represented by a polyline composed of edges and vertices. The 2D rest state of each segment is implicitly parameterized by a length per segment that is distributed uniformly to each edge and a turning angle per vertex that defines the discrete curvature of the polyline. These length and curvature values constitute the design parameters that are optimized. The simulation variables are vertex positions and material frame angles of each rod as well as the position, orientation, and angle of each crossing. These variables determine the 3D equilibrium state of the weave.

Ribbon Crossings. Even though the joint model proposed for X-shells in [Panetta et al. 2019] was originally designed for pin-jointed straight bars, we found it well suited to model curved weaving crossings. This might seem counter-intuitive at first because we want to allow ribbons to slide along each other during the optimization to reduce elastic energy, while an X-shell is composed of beams connected with fixed pin joints. However, sliding does occur naturally in our setting, because the lengths of rod segments between crossings are free variables in the optimization: if advantageous to reduce the energy, one segment can lengthen while its adjacent segment can shorten, effectively letting a ribbon slide along its counterpart at the crossing. By construction, such sliding cannot lead to cross-overs, as the topology of G is fixed and the segment lengths are constrained to remain above a minimal positive value. Another distinct advantage of this model is that ribbons are implicitly constrained to lie flat on top of each other at crossings, which generally leads to more stable weaves. To account for the thickness of ribbons and their alternating over/under crossings, we extend the X-shell joint model to apply a positional offset to the participating centerlines.

6 OPTIMIZATION OBJECTIVE

In this section, we formulate the objective function of our inverse optimization for curved weaving. We use a reduced notation here to simplify the exposition. A detailed and more implementation-friendly description is provided separately in the supplemental material. Our algorithm is defined as a nested optimization that interleaves design parameter improvements with equilibrium solves for fixed design parameters. We first discuss the objective terms of these two optimizations, then present our multi-stage numerical solver in section 7.

6.1 Equilibrium Objective

As mentioned above, the planar rest states of the ribbons are defined by per-segment length variables and per-vertex in-plane turning angles that are stored in the design parameter vector $\mathbf{p}$. For a fixed design $\mathbf{p}$, we solve for its equilibrium state $\mathbf{x}^*_\mathbf{p}$ by minimizing the elastic energy of the ribbons:

$$\mathbf{x}^*_\mathbf{p} = \underset{\mathbf{x}}{\operatorname{argmin}}\, E(\mathbf{x}, \mathbf{p}) + T(\mathbf{x}), \tag{1}$$

where $E(\mathbf{x}, \mathbf{p}) = E_s(\mathbf{x}, \mathbf{p}) + E_b(\mathbf{x}, \mathbf{p}) + E_t(\mathbf{x}, \mathbf{p})$ sums the stretching, bending, and twisting terms of all rod segments, respectively, as defined in [Bergou et al. 2010, 2008]; see also supplemental material. $T(\mathbf{x})$ is a surface closeness term defined below in Equation 3 that is added here with a low weight $\beta_T = 10^{-5}$ to factor out the global rigid motion.

Note that this optimization is not an accurate physical simulation for *arbitrary* woven structures. Since the rest length and curvature parameters are fixed during this solve, we are effectively computing the equilibrium under additional rotational pin constraints at each crossing (like in X-shells) that can hold the ribbons in artificial high-energy configurations. However, as mentioned above, ribbon sliding is implicitly handled in the outer design optimization discussed below, ensuring any artificial forces applied by these pin constraints effectively vanish in our optimized designs.

6.2 Design Parameter Objective

The goal of the design optimization is to find optimal parameters $\mathbf{p}$ so that the resulting equilibrium weave $\mathbf{x}^*_\mathbf{p}$ has low elastic energy, is physically meaningful, and best approximates the target surface S. We formulate this objective as

$$J(\mathbf{p}) = E(\mathbf{x}^*_\mathbf{p}, \mathbf{p}) + T(\mathbf{x}^*_\mathbf{p}) + C(\mathbf{x}^*_\mathbf{p}) + R(\mathbf{p}), \tag{2}$$

where E measures the elastic energy at equilibrium, T denotes a surface closeness term, C promotes beneficial contact forces, and R is a regularization term.

Closeness Term. We measure the distance between the woven structure and the target design surface as

$$T(\mathbf{x}) = \frac{\beta_T}{l_0^2} ||\mathbf{x}_{\text{pos}} - P_{S,G}(\mathbf{x}_{\text{pos}})||^2_W, \tag{3}$$

where $\mathbf{x}_{\text{pos}} = [\mathbf{x}_r\ \mathbf{x}_c] \subset \mathbf{x}$ extracts the positions $\mathbf{x}_r$ of the rod centerline vertices and the locations $\mathbf{x}_c$ of ribbon crossings from the simulation variables $\mathbf{x}$. The function $P_{S,G}(\mathbf{x}_r)$ computes the projection onto S, while $P_{S,G}(\mathbf{x}_c)$ returns the initial crossing locations specified in G (that are embedded in S). To avoid scale dependencies,

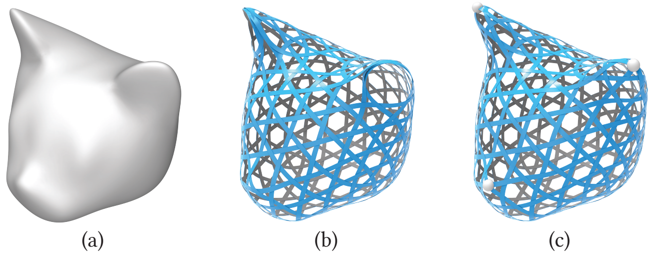

Fig. 10. The surface closeness term T controls the alignment with the input surface (a) and can be adapted with spatially varying weights. Uniform weights do not preserve the features well around the ears and nose of the cat (b). A more satisfactory result is obtained when increasing the weights for the locations indicated by the white spheres by a factor of 100 (c).

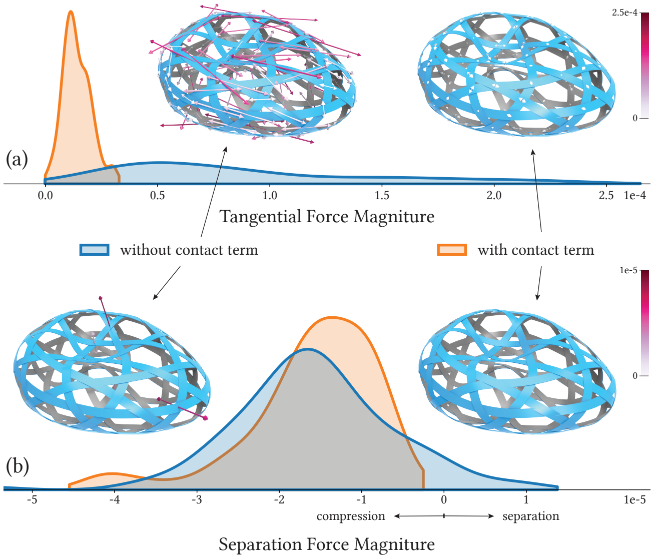

Fig. 11. Without contact force optimization, ribbons can have large tangential forces at crossings (a) that cannot be compensated by friction, or even positive separation forces in the final equilibrium state (b). With the contact term, a more stable weave without ribbon separation is found. The plots show density histograms of force magnitudes. Arrows indicate the force vectors at crossings separated into tangential (a) and normal (b) components. At equilibrium, the forces exerted by ribbon r_i on r_j are balanced by opposite forces exerted by ribbon r_j on r_i in our crossing model.

we normalize the closeness term with the length l_0 of the bounding box diagonal of the target surface. The weight β_T controls the trade-off between surface fitting and the other performance considerations of the final weave. The diagonal matrix W allows specifying the relative importance of accurately approximating different regions of the input surface (see also Figure 10).

Contact Term. As discussed above, a woven structure gains structural stability through frictional interactions between ribbons at their crossings. A stable weave thus requires ribbons to push against each other at their contact point and experience low tangential forces that can be compensated by static friction. So far, the optimization does not explicitly consider contact forces, which can result in the final physical ribbons sliding or even separating at their crossing, as illustrated in Figure 11(a). To address this issue, we introduce an objective term to minimize tangential forces and promote compressive contact forces at ribbon crossings. section 7 will describe an alternative approach to improve contacts based on flipping the over-under relation at certain crossings.

Consider a crossing of two ribbons r_i and r_j. We can compute the force of ribbon r_i acting on r_j at their crossing as the derivative of the elastic energy with respect to the crossing position $\mathbf{c}_{ij}$:

$$\mathbf{f}_{ij} = \frac{\partial}{\partial \mathbf{c}_{ij}} E_{r_j}(\mathbf{x}, \mathbf{p}), \tag{4}$$

where E_{r_j} sums the elastic energy of only the ribbon segments belonging to r_j. From $\mathbf{f}_{ij}$, we can extract the normal *separation* force as

$$f_{ij}^n := s_{ij} \mathbf{n}_{ij} \cdot \mathbf{f}_{ij}.$$

Here, $s_{ij} \in \{-1, 1\}$ denotes whether ribbon r_i passes over (+1) or under (−1) ribbon r_j with respect to the outward pointing crossing normal $\mathbf{n}_{ij}$. Consequently, positive values of this scalar force measure correspond to forces pulling the ribbons apart. The squared tangential force magnitude can be computed as

$$\left(f_{ij}^t\right)^2 := \|\mathbf{f}_{ij}\|^2 - \left(f_{ij}^n\right)^2.$$

Finally, our contact optimization term is formulated as:

$$C(\mathbf{x}, \mathbf{p}) := \frac{1}{2} \sum_{ij} w_n \left(f_{ij}^n - \epsilon_n\right)_+^2 + w_t \left(f_{ij}^t\right)^2,$$

where $(\cdot)_+$ clamps its argument to positive values, ϵ_n is an activation threshold for the separation force penalty, and w_n and w_t are weights for the normal and tangential terms, respectively. Note that setting ϵ_n slightly *negative* will promote a strictly compressive force rather than just eliminating tensile forces. As shown in Figure 11, the contact term can significantly reduce tangential forces and avoids the separation of ribbons at crossings.

Regularization Term. We introduce additional regularization on the design parameters to better control the final shape of ribbons. In particular, we favor short and smoothly curving ribbons by minimizing length and curvature variation:

$$R(\mathbf{p}) = \beta_l \|\mathbf{p}_l\|_1 + \frac{\beta_\kappa}{2} \mathbf{p}_\kappa^T L \mathbf{p}_\kappa \tag{5}$$

Here $\mathbf{p}_l \subset \mathbf{p}$ represents all per-segment length parameters, while $\mathbf{p}_\kappa \subset \mathbf{p}$ accumulates all per-vertex turning angles of the ribbons' rest states. L is a 1D uniform Laplacian matrix, which means the smoothing term is proportional to the total squared difference in turning angle across all ribbon edges. The weights β_l and β_κ are design controls exposed to the user. Figure 12 illustrates the effect of regularization.

7 MULTI-STAGE SOLVER

The objective function Equation 2 defines a challenging nonlinear, nonconvex optimization problem. Rather than enforcing the optimality conditions for Equation 1 as a nonlinear equality constraint

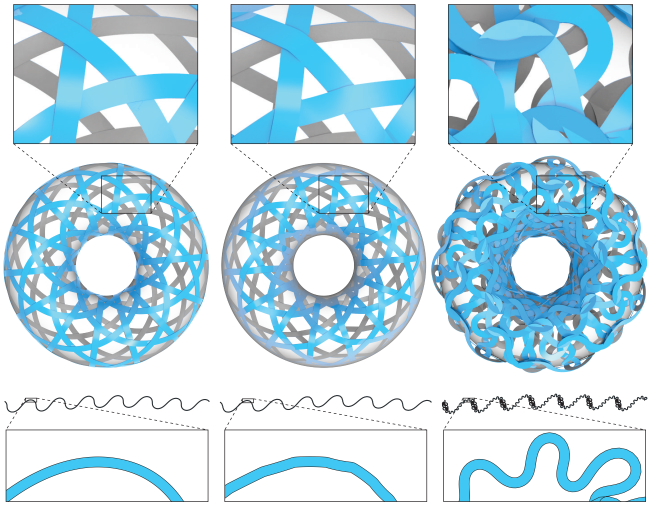

Fig. 12. The regularization terms help stabilize the optimization and improve the quality of ribbon shapes (a). Without curvature regularization, the optimization favors piecewise straight ribbons with sharp kinks that might be undesirable (b). Without length regularization, ribbons can become very curvy and self-intersecting (c). The bottom images show the planar ribbon rest states.

in a large simultaneous optimization for $\mathbf{x}$ and $\mathbf{p}$, we opt for a reduced optimization over $\mathbf{p}$ alone wherein the forward equilibrium minimization problem is solved in the inner loop for each candidate design $\mathbf{p}$. We perform exact, analytic first- and second-order sensitivity analysis to account for the changing equilibrium state $\mathbf{x}^*_\mathbf{p}$ when computing first and second derivatives of J with respect to $\mathbf{p}$ (see also supplemental material Section 2 for more details). This ensures surface deviations and crossing forces considered by the optimizer are always physically meaningful and that the weave is in *stable* equilibrium, which is not guaranteed merely by satisfying the force balance constraint.

This nested optimization relies on being able to robustly and quickly solve the equilibrium problem for each $\mathbf{p}$, which turns out to be problematic for the poor designs often considered at early optimization iterations. As one of the key goals for our design tool is not requiring the user to provide good initial ribbon rest curvatures and lengths (which are generally difficult to find manually), we propose a simplified initial optimization stage that rapidly converges to a reasonable design from a naïve initialization—straight ribbons with segment rest lengths taken from the Euclidean lengths of edges in G (see also Figure 7). Furthermore, we found it beneficial for convergence to include the highly nonlinear contact term only after an optimal design is found for the fitting objective. We therefore propose a three-stage optimization algorithm.

Stage I. The initial woven structure with straight ribbons tends to be poorly behaved and has numerous barely stable equilibria featuring twisted and buckled ribbons. This slows down the equilibrium solve and thwarts sensitivity analysis as a small change to the design parameters can cause ribbons to pop from one buckled configuration to another, making the objective discontinuous.

However, we note that by dropping the contact and surface closeness terms from $J(\mathbf{p})$, we obtain a simplified objective where the simulation variables appear only in the elastic energy term. Hence, if we optimize just this objective over both $\mathbf{x}$ and $\mathbf{p}$ without explicitly enforcing equilibrium, the result will be a smooth, low-energy structure *in stable equilibrium.* To ensure this low-energy structure is also close to the target surface, we add pin constraints holding the crossings at their original positions on the target surface (effectively applying additional artificial forces). Crucially, we avoid solving equilibrium problems for poorly behaved designs in this formulation. Stage I of the optimization therefore solves:

$$\mathbf{x}^I, \mathbf{p}^I = \underset{\substack{\mathbf{x},\mathbf{p} \text{ s.t. } \mathbf{p}_l > \epsilon \\ \mathbf{x}_c = P_{S,G}(\mathbf{x}_c)}}{\operatorname{argmin}} \; E(\mathbf{x}, \mathbf{p}) + R(\mathbf{p}). \tag{6}$$

We constrain the segment lengths $\mathbf{p}_l$ to remain above a small positive threshold ϵ to avoid ribbon cross-over. This optimization yields a first significant change in the ribbon rest lengths and curvatures as illustrated in Figure 13. Unfortunately, $\mathbf{x}^I$ is only an equilibrium under the additional forces artificially holding ribbon crossings in place; once we release these constraints, the weave will deviate from the target surface. However, the true equilibrium $\mathbf{x}^*_{\mathbf{p}^I}$ is now efficiently computable and differentiable.

An alternative initialization method is to project the edges of the input topology graph onto the target surface and assign the geodesic curvature of the projection curves to the ribbons. However, we find that this method neither speeds up nor improves the subsequent optimization because the feasible solution space of Equation 6 contains this initialization. Moreover, our current initialization method does not depend on the mesh quality of the target surface. Our framework can also find optimal woven structures for different objectives other than shape approximation.

Stage II. Given the solution of stage I, we now remove the constraints on crossing positions and integrate the full surface closeness term:

$$\mathbf{p}^{II} = \underset{\mathbf{p} \text{ s.t. } \mathbf{p}_l > \epsilon}{\operatorname{argmin}} \; E(\mathbf{x}^*_\mathbf{p}, \mathbf{p}) + T(\mathbf{x}^*_\mathbf{p}) + R(\mathbf{p}). \tag{7}$$

This allows the ribbon crossings to move freely and ribbons to slide along each other to reduce the equilibrium energy as illustrated in Figure 13. We note that this objective indirectly encourages the reduction of tangential forces applied by the imaginary pins in our simulation model since any work done by these forces increases E.

Stage III. At the end of stage II we evaluate the contact forces Equation 4 acting on each ribbon crossing. If we observe a separation of ribbons, we run the final stage that now uses the full objective function Equation 2 including the contact term:

$$\mathbf{p}^* = \mathbf{p}^{III} = \underset{\mathbf{p} \text{ s.t. } \mathbf{p}_l > \epsilon}{\operatorname{argmin}} \; E(x^*_\mathbf{p}, \mathbf{p}) + T(\mathbf{x}^*_\mathbf{p}) + C(\mathbf{x}^*_\mathbf{p}) + R(\mathbf{p}). \tag{8}$$

Figure 13 shows a typical example of the convergence behavior of our solver. As can be observed, stage I quickly progresses towards a solution with good surface fit and significantly reduced elastic energy as the rest curvature of the ribbons increases (green curve in (d)). However, once the crossing position constraints are released, the true equilibrium state of the structure can still deviate from the target surface. In this example, the negative mean curvature region

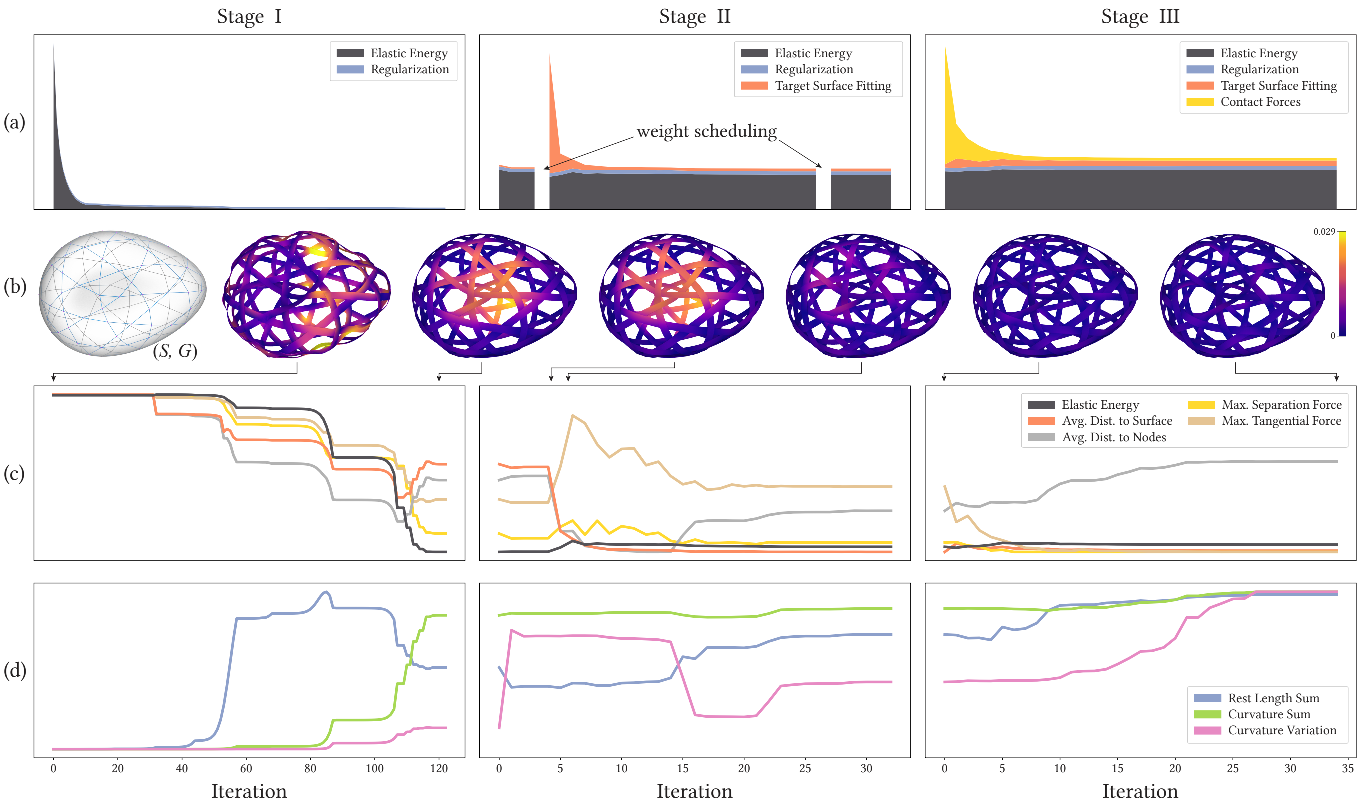

Fig. 13. Typical convergence behavior of our multi-stage optimization. (a) shows the objective function as a normalized stacked graph to indicate the relative importance of each objective term. The gaps in stage II correspond to weight changes in our weight scheduling scheme. (b,c) show physical and geometric quantities computed for the 3D equilibrium state of the weave without positional constraints on crossing nodes. The color of the structures in (b) encodes the distance to the target surface, which is computed relative to the bounding box diagonal. *Avg. Dist. to Nodes* indicates how ribbon crossings evolve from the initial position specified in the topology graph. (d) shows how geometric quantities of the 2D rest state of the ribbons change during the optimization, i.e. the aggregate length and in-plane curvature of the ribbons as well as their total variation of curvature.

of the target surface is not well approximated at the end of stage I. In stage II, we apply a 3-phase weight scheduling scheme where an initially high surface attraction weight is progressively reduced. Specifically, we set β_T of Equation 3 in the equilibrium objective Equation 1 to $[100, 10^{-3/2}, 10^{-5}]$ for the three phases as indicated by the gaps in stage II in (a). These empirically selected values worked well in all our examples. As can be observed, the distance of the woven structure to the target surface decreases significantly in this stage. Stage III generally leads to only minor changes in ribbon geometry. Nevertheless, the reduction in tangential forces and separation forces can be significant.

Flipping Ribbon Crossings. The continuous contact optimization of stage III is not always successful or efficient at eliminating separation forces from all ribbon crossings while keeping the equilibrium state sufficiently close to the target surface. We offer a second, alternative strategy to improve the stability of the weave by altering the over-under relations at crossings.

Initially, any two consecutive crossings along a ribbon have alternating over-under relations. This regularity is in general conducive to stable crossings and is often preferred for reasons of aesthetics and ease of weaving. However, for certain weaving topologies and target shapes, deviating from the regular pattern can help avoid ribbon separation at crossings.

Our algorithm is very simple: We first detect all crossings with separation forces. Then we flip the over-under relation for these crossing and re-run the equilibrium solve. If we still observe separation forces at crossings, we iterate. Intuitively, the separation forces will become compressive forces after the switch of the over-under relation. However, this is not necessarily the case due to the global coupling of the elastic forces. Therefore, we solve for the equilibrium state with the flipped crossings and recompute the contact forces at all crossings; the algorithm only proceeds with the flipping operation if it actually decreases the total separation force magnitude. This greedy algorithm is not guaranteed to terminate, so we limited the number of iterations and provide additional user control to interactively select ribbons for flipping if desired. Figure 14 shows an example where our method successfully resolved all ribbon separation issues as well as a failure case. At difficult crossings where neither Stage III nor flipping can remove the separation forces, we can stabilize the ribbons with pins as a practical remedy.

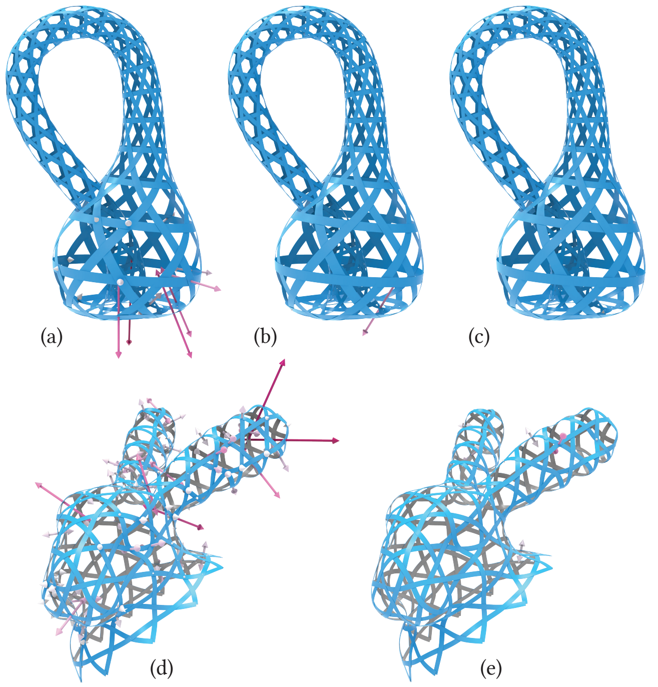

Fig. 14. Iterative Contact handling: After stage II of the optimization, we observe significant separation forces (a,d). As an alternative to contact optimization, we show the result of the flipping procedure after two iterations (b) and three iterations (c), where all separation forces have been eliminated for the Klein bottle. For the bunny, the algorithm fails to find a solution eliminating all separation forces (e).

8 RESULTS AND DISCUSSION

We have integrated our inverse optimization algorithm into an end-to-end computational design framework for curved weaving. Please refer to the supplemental material for a detailed description of the implementation, corresponding source code, as well as all parameter settings to reproduce the results shown in the paper.

In order to produce physical models, we integrate the length and curvature angles found by our optimization algorithm to compute vector curves that define the boundaries of the planar curved ribbons. These can directly serve as input to digital fabrication machines or be printed on paper to be cut by hand. In all our examples, a laser cutter (Trotec Speedy 400) is used to fabricate the ribbons using polyethylene (PETE) sheets (Plastic Shim Pack DM1210, Partwell Group, United Kingdom). This material is relatively smooth and leads to low friction between the ribbons in the weave (see also Figure 6 and accompanying video). We manually weaved all the shown models using the visualization web application provided in supplemental material to guide the incremental interlacing of ribbons. Ribbon crossings at open boundaries are connected with pins to allow rotation around the contact vertex as modeled in our optimization. We also reconnect the endpoints of closed-curve ribbons during weaving (see Figure 8). Weaving time depends on model complexity and the weaver's experience. For example, the owl (Figure 4) took a novice weaver less than two hours, and the cat (Figure 10) and bunny (Figure 8) took around three to four hours. We found the weaving process engaging and envision people weaving interesting 3D shapes at home as a recreational activity, analogous to puzzles or model building.

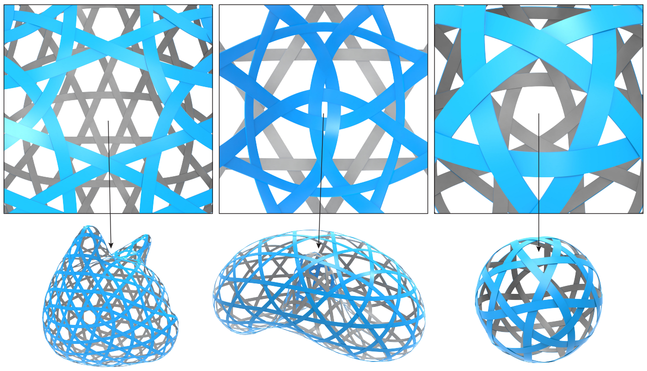

Fig. 15. Singularities can be used control the weaving pattern and reduce in-plane curvature of ribbons in highly curved regions of the design surface. They can also be required to satisfy global topological constraints.

Figure 1 shows a series of physical prototypes that we have optimized and fabricated using our approach with some statistics provided in Table 1. Please also refer to the supplemental material for additional visualizations, 3D models, and complete 2D cutting plans for all of the results shown in the paper.

The Klein bottle (see also Figure 7 and Figure 14) is an example of a complex double-curved surface that cannot be well approximated with straight ribbons only as illustrated in Figure 3(b). Notably, our result has a perfectly regular topology without any singularities. For aesthetic reasons, we adapted the ribbon width automatically to match the inter-ribbon spacing. Our simulation framework accurately models the varying ribbon width. In this weave, each ribbon forms a closed loop. Curiously, even though the Klein bottle is non-orientable, none of the ribbons is a Möbius strip. Ribbons loop around the surface multiple times to avoid a discontinuous jump in orientation at their connection.

Topology and Geometry. As mentioned before, traditional weaving with straight ribbons requires topological singularities in the weaving pattern to approximate curved surfaces. These often lead to undesirable local curvature concentrations in the woven structure (Figure 3). Our optimized curved ribbons do not suffer from this deficiency and can in general operate on a much broader range of weaving topologies.

Surfaces with Euler characteristic zero such as the torus and Klein bottle, for example, do not require any singularities to be approximated accurately and smoothly. On the other hand, we can use singularities to control the weaving pattern or reduce in-plane curvature of ribbons in highly curved regions of the design surface as illustrated in Figure 15. Importantly, any geometric distortions caused by topological singularities can be compensated by ribbon rest curvature, so that a smooth appearance is preserved.

The flexibility to optimize different weaving patterns is demonstrated in Figure 16, where biaxial and triaxial weaving patterns are

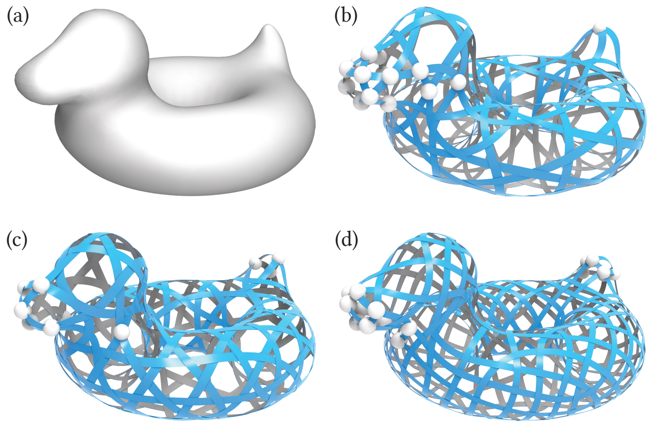

Fig. 16. The same input target shape (a) optimized for different weaving patterns: a hand-designed triaxial input topology graph (b) and two automatically computed graphs for a triaxial (c) and biaxial (d) weaving pattern. The manually placed white spheres indicate a 100× higher closeness term weight to enforce better feature preservation at the bill and tail.

used on the same input target model. We manually created a triaxial input topology graph using Rhinoceros 3D [McNeel et al. 2010]. The auto-generated graphs are produced by first triangulating (for triaxial pattern) or quadrangulating (for biaxial pattern) the input surfaces using Instant Meshes [Jakob et al. 2015]. Then a graph node is created at each mesh edge midpoint, and these nodes are connected in cyclic order around each face. Here we illustrate also how to employ spatially varying fitting weights to control feature preservation of the final weave (see also Figure 10).

Figure 18 highlights an additional benefit of curved ribbons: for a fixed weaving topology, we can continuously blend between shapes, here illustrated by a cat-to-sphere morph. When using straight ribbons, this geometry change could only be accommodated by introducing topological singularities, leading to localized curvature concentrations and discontinuous jumps in the morphing sequence.

Figure 19 illustrates the potential of our method for applications in architecture or furniture design. Compared to purely geometric methods, our physics-based simulation framework offers additional advantages. For example, we can easily integrate and account for additional constraints, e.g. gravitational or other loading, that can be relevant in such applications.

8.1 Validation

To systematically evaluate the accuracy of our inverse design algorithm, we scanned all our physical prototypes using photometric reconstruction provided by the Agisoft Metashape software. Figure 20 shows on some examples how our simulation accurately predicts the final fabricated shape. The complete set of quantitative comparisons is provided in the supplemental material. As can be seen in Table 1, the maximal deviation of the physical model from the input design surface is between 1% and 4% of the bounding box diagonal. These measurements confirm that our computational framework can be used for exploring design alternatives before fabrication, avoiding time-consuming and costly prototyping iterations.

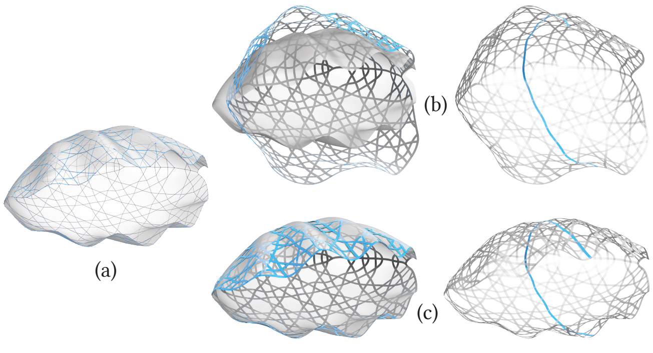

Fig. 17. A failure case for our approach. When trying to approximate the input surface shown in (a) the weave settles into an equilibrium state far from the desired target (b). In particular, ribbons traversing across the model, as the one highlighted on the right, exert high bending forces, pulling the structure open. Only when explicitly fixing the boundary curve can we achieve a faithfully approximation (c).

8.2 Limitations

A general limitation of our approach is that curved ribbons are less suited for certain natural materials that are extensively used in traditional basket weaving, such as wood or bamboo. These materials have clearly defined fiber directions that lead to highly anisotropic bending behavior. Our approach is more suited for materials such as paper, plastics, or composites, where bending behavior is more isotropic.

Another inherent limitation is that curved ribbons, in general, cannot be packed without gaps, leading to potential waste when cutting ribbons from sheet material. Long and curved ribbons also tend to exceed the laser cutting machine's dimensions and have in-plane self-intersections. Hence, we need to split the ribbons for fabrication (see also Figure 8). We currently perform both the splitting and packing processes manually. Algorithms to optimize the decomposition and arrangement of ribbons for fabrication can mitigate this drawback [Limper et al. 2018].

Figure 17 shows a failure case of our approach. In particular for surfaces with large free boundaries, the elastic forces of the ribbons can sometimes lead to close-to-isometric deformations of the equilibrium state away from the desired target surface. Such cases either require additional constraints, e.g. in form of a rigid boundary, changes to material properties, e.g. reducing the bending stiffness of ribbons, or a re-design of the ribbon topology.

Some input geometries, in particular with complex boundaries or thin features, can cause difficulties for our optimization. For example, the ear of the bunny or the tail of the bird in Figure 20 show relatively large deviations from the input surface. More accurate results could potentially be achieved with a denser weaving graph, but we did not verify this conjecture yet.

We do not explicitly simulate the effect of friction and instead rely on the minimization of tangential forces at ribbon crossings to ensure stability of the weave. Our contact optimization cannot always guarantee that ribbons experience only compressive forces at their crossings, i.e., that the two ribbons always push against each other. This can cause the final equilibrium shape to deviate

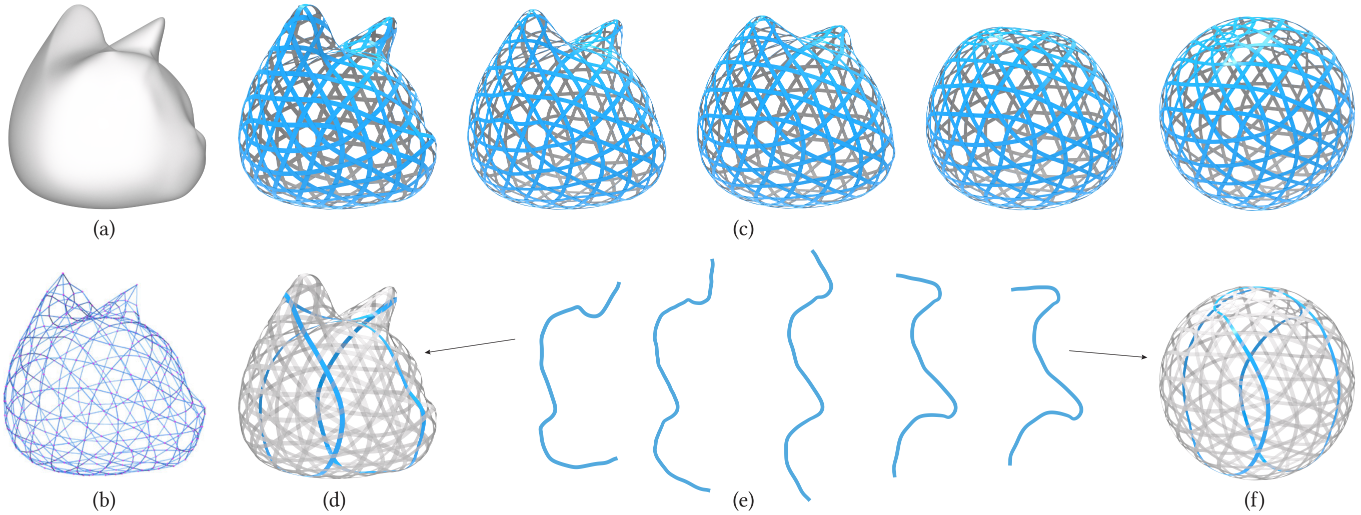

Fig. 18. A morphing sequence from cat to a sphere. The graph topology (b) is kept fixed as the input geometry (a) is smoothly morphed towards the sphere. For each deformed target state, we run our optimization to compute the corresponding curved weavings (c). For a single highlighted ribbon (d,f) we illustrate how the 2D rest geometry changes continuously in the morphing sequence (e).

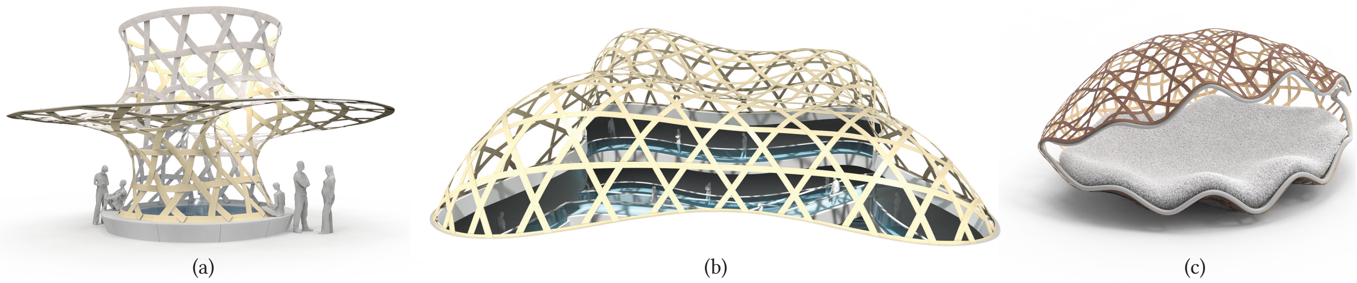

Fig. 19. Application case studies for optimized curved weaving: A pavilion (a), a roof structure (b), and furniture (c).

from the simulated prediction. In our current system, we handle this issue by providing visual feedback to the user that highlights all crossings with tensile forces so appropriate editing actions can be taken. We found, however, that such cases are rare and that the resulting inaccuracies were generally not too significant.

9 CONCLUSION AND FUTURE WORK

Curved ribbons offer a rich design space for weaving 3D surface structures. Even though often not obvious on the final woven model, the geometry of the curved ribbons can be highly complex and unintuitive. Effective design thus requires advanced computational methods to optimize ribbon geometry and accurately predict the final equilibrium structure. Our inverse design algorithm provides a solution to this challenging problem, opening the door to the entirely new applications of woven geometries for industrial and consumer products, artistic installations, or architectural designs, for example.

An exciting path for future work is to further investigate the interplay between topological singularities and ribbon curvature. Currently we assume the singularity structure is fixed and provided as input. However, allowing singularities to be dynamically introduced or removed, for example driven by user input or to reduce stress in the structure, could allow for a more powerful design exploration process. We also did not yet investigate how to create effective weaving instructions, which will be important especially for novice users. Finally, actuated curved ribbons could be an interesting way to design shape-shifting structures.

ACKNOWLEDGMENTS

We are grateful to Pedro Reis and Changyeob Baek for insightful discussions. We also thank the anonymous reviewers for their valuable feedback. This research was supported by the NCCR Digital Fabrication, funded by the Swiss National Science Foundation (NCCR Digital Fabrication Agreement #51NF40-141853) and the SNF Award (FNS 514543 / CF 1156).

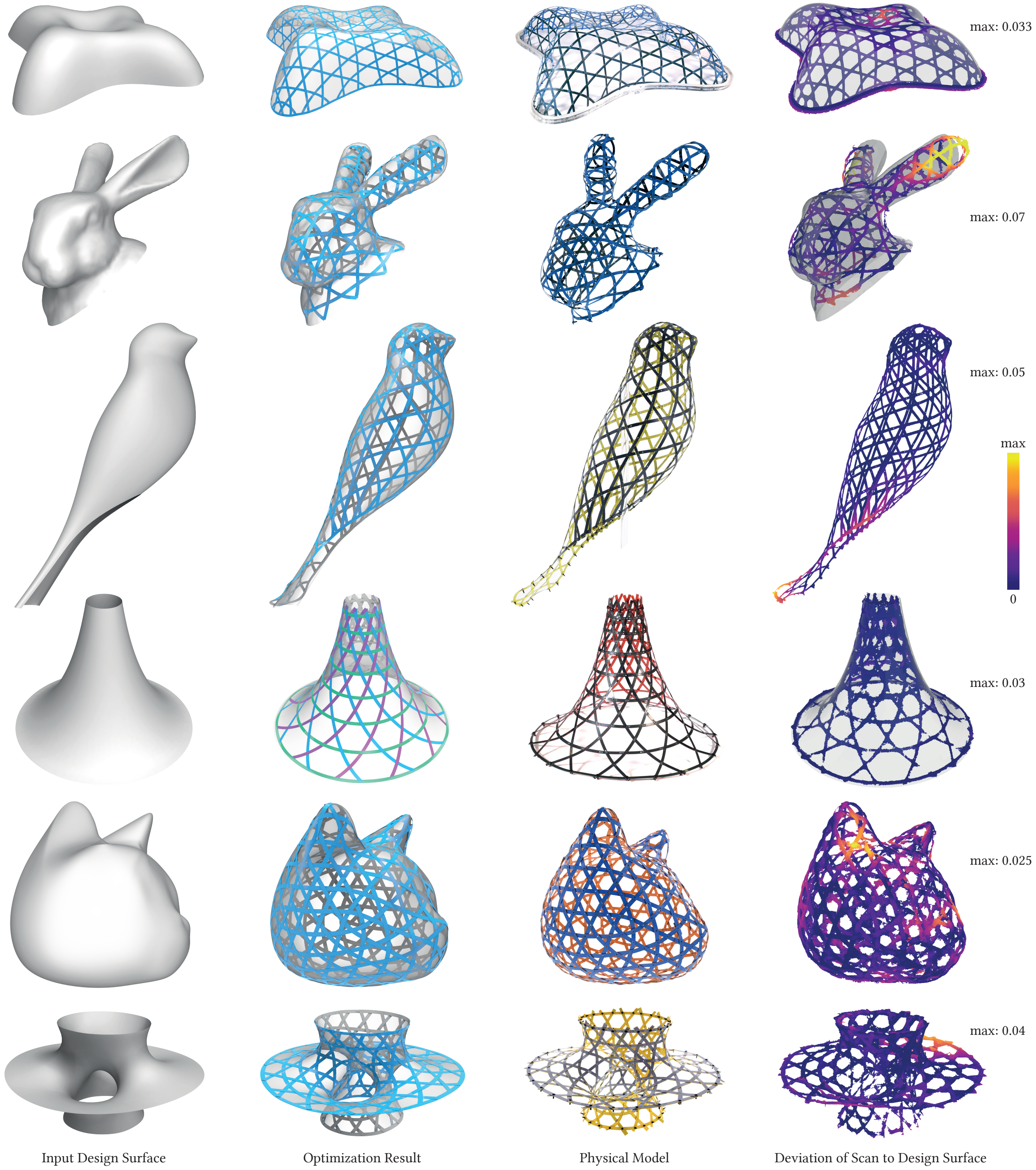
max: 0.033
max: 0.07
max: 0.05
max
0
max: 0.03
max: 0.025
max: 0.04
Input Design Surface
Optimization Result
Physical Model
Deviation of Scan to Design Surface

Fig. 20. Validation of our inverse design pipeline with physical prototypes. All models have been scanned using photometric stereo. Max deviation is indicated as a fraction of the bounding box diagonal.

Table 1. Statistics of the examples shown in the paper. *# Crs* is the number of ribbon crossings and *# Rib.* shows the number of ribbons in the weave (in parentheses, the number of physical ribbons after splitting to fit into the laser cutter). $|\mathbf{x}|$ is the number of DoFs in the 3D equilibrium simulation, $|\mathbf{p}|$ is the number of DoFs of the planar ribbon rest states, i.e. the design variables we optimize for. Timings for stage I-III and Total are in (hour:)min:sec measured on a Linux workstation with a 64-Core AMD Ryzen Threadripper 3990X Processor and 128GB of RAM. We allocate 6 threads to our optimization solver. *Sim. Fit* and *Scan Fit* measure the maximum distance relative to the model bounding box between the target surface and the simulated weave and scanned prototype, respectively.

Model (Figures)	# Crs.	# Rib.	$\lvert\mathbf{x}\rvert$	$\lvert\mathbf{p}\rvert$	Stage I	Stage II	Stage III	Total	Sim. Fit	Scan Fit
Sphere (15)	90	10 (10)	13,230	3’600	00:01	00:10	-	00:11	0.0031	-
Teardrop (11, 13)	120	12	17640	4800	00:06	01:43	06:01	07:50	0.0062	-
Torus (12)	252	16 (22)	37044	10080	00:13	02:53	-	03:06	0.0025	0.01510
Pseudosphere (1, 20)	264	30 (32)	37290	10120	00:22	21:57	-	22:19	0.007	0.01436
Duck (16(c))	300	5	44100	12000	01:03	06:58	05:25	13:26	0.0125	-
Duck (16(b))	303	10	44541	12120	00:41	13:15	15:38	29:33	0.0075	-
Duck (16(d))	352	3 (45)	51744	14080	02:08	12:06	24:42	38:56	0.0085	0.0145
Bunny (1, 8, 20)	315	13 (26)	45477	12360	01:19	40:18	18:06	59:43	0.0127	0.0633
Bird (1, 15, 20)	326	17 (35)	46749	12700	00:26	25:40	2:11:21	2:37:27	0.0081	0.0217
Bean (15)	372	14	54684	14880	00:19	10:01	22:40	32:60	0.0019	-
Owl (4)	384	32 (42)	54240	14720	03:01	29:01	01:59	34:01	0.0163	0.0400
Costa (1, 9, 19, 20)	396	48 (60)	55452	15040	01:49	11:49	-	13:38	0.0075	0.0186
Lilium (1, 19, 20)	488	45 (56)	68700	18640	00:27	18:37	1:48:28	2:07:31	0.0045	0.0220
Cat A (1, 10, 18, 15)	516	14 (37)	75852	20640	01:02	16:59	19:14	37:15	0.0115	0.0130
Cat B (18)	516	14	75852	20640	02:00	15:15	17:16	34:30	0.0074	-
Cat C (18)	516	14	75852	20640	01:18	36:09	1:07:18	1:44:45	0.0025	-
Cat D (18)	516	14	75852	20640	01:32	24:39	-	26:11	0.0015	-
Cat E (18)	516	14 (39)	75852	20640	01:23	18:54	-	20:17	0.0014	0.0168
Klein Bottle (1, 7, 14)	540	36 (67)	79380	21600	03:39	29:45	21:47	55:11	0.0021	0.0182
Clam (17, 19)	674	43	96318	26160	03:04	38:44	09:35	51:23	0.0095	-

REFERENCES

Ergun Akleman, Jianer Chen, Qing Xing, and Jonathan L Gross. 2009. Cyclic plain-weaving on polygonal mesh surfaces with graph rotation systems. *ACM Transactions on Graphics (TOG)* 28, 3 (2009), 1–8.

Nicholas Fox Weber Albers, Anni, Manuel Cirauqui, and T'ai Smith. 2017. *On Weaving: New Expanded Edition.* Princeton University Press, Princeton, NJ, USA.

Phil Ayres, Alison Grace Martin, and Mateusz Zwierzycki. 2018. Beyond the Basket Case: a principled approach to the modelling of Kagome weave patterns for the fabrication of interlaced lattice structures using straight strips. In *Advances in Architectural Geometry 2018.* Chalmers University of Technology, 72–93.

Phil Ayres, Adam Orlinski, Moritz Heimrath, Soraya Bornaz, and Alison Martin. 2020. Architectural Scale Kagome Weaving: Design Methods and Fabrication Concepts. In *Fabricate Conference Proceedings.*

Changyeob Baek, Alison Martin, Samuel Poincloux, Tian Chen, and Pedro Reis. 2020. How to weave a perfect sphere with curved strips. *arXiv* (2020).

B.K. Behera and P.K. Hari. 2010. *Woven Textile Structure: Theory and Applications.* Elsevier Science. https://books.google.ch/books?id=oJVwAgAAQBAJ

Miklós Bergou, Basile Audoly, Etienne Vouga, Max Wardetzky, and Eitan Grinspun. 2010. Discrete viscous threads. *ACM T Graphic* 29, 4 (2010), 116.

Miklós Bergou, Max Wardetzky, Stephen Robinson, Basile Audoly, and Eitan Grinspun. 2008. Discrete elastic rods. *ACM T Graphic* 27, 3 (2008), 63.

Amit H. Bermano, Thomas Funkhouser, and Szymon Rusinkiewicz. 2017. State of the Art in Methods and Representations for Fabrication-Aware Design. *Comput. Graph. Forum* 36, 2 (May 2017), 509–535. https://doi.org/10.1111/cgf.13146

Marcel Campen and Leif Kobbelt. 2014. Dual Strip Weaving: Interactive Design of Quad Layouts Using Elastica Strips. *ACM Trans. Graph.* 33, 6, Article 183 (Nov. 2014), 10 pages. https://doi.org/10.1145/2661229.2661236

Weikai Chen, Xiaolong Zhang, Shiqing Xin, Yang Xia, Sylvain Lefebvre, and Wenping Wang. 2016. Synthesis of Filigrees for Digital Fabrication. *ACM Trans. Graph.* 35, 4, Article 98 (July 2016), 13 pages. https://doi.org/10.1145/2897824.2925911

Gary P. T. Choi, Levi H. Dudte, and L. Mahadevan. 2019. Programming shape using kirigami tessellations. *Nature Materials* 18, 9 (2019), 999–1004. https://doi.org/10.1038/s41563-019-0452-y

Bailin Deng, Helmut Pottmann, and Johannes Wallner. 2011. Functional webs for freeform architecture. In *Computer Graphics Forum*, Vol. 30. Wiley Online Library, 1369–1378.

Levi Dudte, Etienne Vouga, Tomohiro Tachi, and Lakshminarayanan Mahadevan. 2016. Programming curvature using origami tessellations. *Nature Materials* 15 (01 2016). https://doi.org/10.1038/nmat4540

I. Fajar and Aswin Indraprastha. 2016. Computational Weaving Grammar of Traditional Woven Pattern. In *Proceedings of the 8th ASCAAD Conference.* 75–84.

Akash Garg, Andrew O Sageman-Furnas, Bailin Deng, Yonghao Yue, Eitan Grinspun, Mark Pauly, and Max Wardetzky. 2014. Wire mesh design. *ACM Transactions on Graphics* 33, 4 (2014).

S. A. Gladman, Elisabetta A. Matsumoto, Ralph G. Nuzzo, L. Mahadevan, and Jennifer A. Lewis. 2016. Biomimetic 4D printing. *Nature Materials* 15 (25 01 2016), 413 EP –. https://doi.org/10.1038/nmat4544

Ruslan Guseinov, Eder Miguel, and Bernd Bickel. 2017. CurveUps: Shaping objects from flat plates with tension-actuated curvature. *ACM Transactions on Graphics (TOG)* 36, 4 (2017), 1–12.

Mike Hansell and Raith Overhill. 2000. *Bird Nests and Construction Behaviour.* Cambridge University Press. https://doi.org/10.1017/CBO9781139106788

Y. Igarashi. 2019. BandWeavy: Interactive Modeling for Craft Band Design. *IEEE Computer Graphics and Applications* 39, 5 (2019), 96–103. https://doi.org/10.1109/MCG.2019.2930930

Wenzel Jakob, Marco Tarini, Daniele Panozzo, and Olga Sorkine-Hornung. 2015. Instant Field-Aligned Meshes. *ACM Trans. Graph.* 34, 6, Article 189 (Oct. 2015), 15 pages. https://doi.org/10.1145/2816795.2818078

Caigui Jiang, Florian Rist, Helmut Pottmann, and Johannes Wallner. 2020. Freeform quad-based kirigami. *ACM Trans. Graphics* 39, 6 (2020). Proc. SIGGRAPH Asia.

Matthew Kaplan and Elaine Cohen. 2003. Computer Generated Celtic Design *(EGRW '03).* Eurographics Association, Goslar, DEU, 9–19.

Martin Kilian, Aron Monszpart, and Niloy J. Mitra. 2017. String Actuated Curved Folded Surfaces. *ACM Trans. Graph.* 36, 4, Article 64a (May 2017), 13 pages. https://doi.org/10.1145/3072959.3015460

Mina Konaković, Keenan Crane, Bailin Deng, Sofien Bouaziz, Daniel Piker, and Mark Pauly. 2016. Beyond Developable: Computational Design and Fabrication with Auxetic Materials. *ACM Trans. Graph.* 35, 4, Article 89 (July 2016), 11 pages. https://doi.org/10.1145/2897824.2925944

Mina Konaković-Luković, Julian Panetta, Keenan Crane, and Mark Pauly. 2018. Rapid deployment of curved surfaces via programmable auxetics. *ACM Transactions on Graphics (TOG)* 37, 4 (2018), 106.

Urszula Lewandowska, Wojciech Zajaczkowski, Stefano Corra, Junki Tanabe, Ruediger Borrmann, Edmondo M Benetti, Sebastian Stappert, Kohei Watanabe, Nellie AK Ochs, Robin Schaeublin, et al. 2017. A triaxial supramolecular weave. *Nature Chemistry* 9, 11 (2017), 1068–1072.

Max Limper, Nicholas Vining, and ALLA SHEFFER. 2018. Box Cutter: Atlas Refinement for Efficient Packing via Void Elimination. *ACM Trans. Graph.* 37, 4, Article 153 (July 2018), 13 pages. https://doi.org/10.1145/3197517.3201328

James Mallos. 2009. How to Weave a Basket of Arbitrary Shape. In *Proceecings of the Eighth Interdisciplinary Conference of The International Society of the Arts, Mathematics, and Architecture.*

Luigi Malomo, Jesús Pérez, Emmanuel Iarussi, Nico Pietroni, Eder Miguel, Paolo Cignoni, and Bernd Bickel. 2018. FlexMaps: Computational Design of Flat Flexible Shells for Shaping 3D Objects. *ACM Trans. Graph.* 37, 6, Article 241 (Dec. 2018), 14 pages. https://doi.org/10.1145/3272127.3275076

Robert McNeel et al. 2010. Rhinoceros 3D, Version 6.0. *Robert McNeel & Associates, Seattle, WA* (2010).

Eder Miguel, Mathias Lepoutre, and Bernd Bickel. 2016. Computational design of stable planar-rod structures. *ACM Transactions on Graphics (TOG)* 35, 4 (2016), 1–11.

Julian Panetta, Mina Konaković-Luković, Florin Isvoranu, Etienne Bouleau, and Mark Pauly. 2019. X-Shells: A new class of deployable beam structures. *ACM Transactions on Graphics (TOG)* 38, 4 (2019), 1–15.

Jesús Pérez, Miguel A. Otaduy, and Bernhard Thomaszewski. 2017. Computational Design and Automated Fabrication of Kirchhoff-Plateau Surfaces. *ACM Trans. Graph.* 36, 4, Article 62 (July 2017), 12 pages. https://doi.org/10.1145/3072959.3073695

Jesús Pérez, Bernhard Thomaszewski, Stelian Coros, Bernd Bickel, José A. Canabal, Robert Sumner, and Miguel A. Otaduy. 2015. Design and Fabrication of Flexible Rod Meshes. *ACM Trans. Graph.* 34, 4, Article 138 (July 2015), 12 pages. https://doi.org/10.1145/2766998

Nico Pietroni, Bernd Bickel, Luigi Malomo, and Paolo Cignoni. 2019. State of the Art on Stylized Fabrication *(SA '19).* Association for Computing Machinery, New York, NY, USA, Article 118, 1 pages. https://doi.org/10.1145/3355047.3359411

Stefan Pillwein, Kurt Leimer, Michael Birsak, and Przemyslaw Musialski. 2020. On Elastic Geodesic Grids and Their Planar to Spatial Deployment. *ACM Trans. Graph.* 39, 4, Article 125 (July 2020), 12 pages. https://doi.org/10.1145/3386569.3392490

Helmut Pottmann, Qixing Huang, Bailin Deng, Alexander Schiftner, Martin Kilian, Leonidas Guibas, and Johannes Wallner. 2010. Geodesic Patterns *(SIGGRAPH '10).* Association for Computing Machinery, New York, NY, USA, Article 43, 10 pages. https://doi.org/10.1145/1833349.1778780

Sohel Rana and Raul Fangueiro. 2015. *Braided Structures and Composites: Production, Properties, Mechanics, and Technical Applications.* CRC Press.

Andrew O. Sageman-Furnas, Albert Chern, Mirela Ben-Chen, and Amir Vaxman. 2019. Chebyshev Nets from Commuting PolyVector Fields. *ACM Trans. Graph.* 38, 6, Article 172 (Nov. 2019), 16 pages. https://doi.org/10.1145/3355089.3356564

Lene Schepper and Anna Schepper. 2014. *Sphere 010 Open.* https://papermatrix.wordpress.com/2014/12/05/sphere-010-open/

Christian Schüller, Roi Poranne, and Olga Sorkine-Hornung. 2018. Shape Representation by Zippables. *ACM Trans. Graph.* 37, 4, Article 78 (July 2018), 13 pages. https://doi.org/10.1145/3197517.3201347

Emmanuel Siéfert, Etienne Reyssat, José Bico, and Benoît Roman. 2019. Bio-inspired pneumatic shape-morphing elastomers. *Nature Materials* 18, 1 (2019), 24–28. https://doi.org/10.1038/s41563-018-0219-x

Ye Tao, Guanyun Wang, Caowei Zhang, Nannan Lu, Xiaolian Zhang, Cheng Yao, and Fangtian Ying. 2017. WeaveMesh: A Low-Fidelity and Low-Cost Prototyping Approach for 3D Models Created by Flexible Assembly *(CHI '17).* Association for Computing Machinery, New York, NY, USA, 509–518. https://doi.org/10.1145/3025453.3025699

Josh Vekhter, Jiacheng Zhuo, Luisa F Gil Fandino, Qixing Huang, and Etienne Vouga. 2019. Weaving Geodesic Foliations. *ACM Trans. Graph.* 38, 4, Article Article 34 (July 2019), 22 pages. https://doi.org/10.1145/3306346.3323043

Qing Xing, Gabriel Esquivel, Ergun Akleman, Jianer Chen, and Jonathan Gross. 2011. Band Decomposition of 2-Manifold Meshes for Physical Construction of Large Structures *(SIGGRAPH '11).* Association for Computing Machinery, New York, NY, USA, Article 58, 1 pages. https://doi.org/10.1145/2037715.2037781

Jonas Zehnder, Stelian Coros, and Bernhard Thomaszewski. 2016. Designing Structurally-Sound Ornamental Curve Networks. *ACM Trans. Graph.* 35, 4, Article 99 (July 2016), 10 pages. https://doi.org/10.1145/2897824.2925888